Catalysis Letters (2025) 155:149
https://doi.org/10.1007/s10562-025-04989-8

Graphitic Nature Governs CO_2 Hydrogenation Reactions on Platinum@Carbon Nanocomposites

Juan Fernando Gómez-Pérez[1,6] · András Sápi[1] · Viola Bíró[1] · Ferenc Farkas[2] · Sebastijan Kovačič[3] · Bence Kutus[4] · Pál Sipos[4] · Henrik Haspel[1,5] · Ákos Kukovecz[1] · Zoltán Kónya[1,5]

Received: 15 June 2024 / Accepted: 21 February 2025 / Published online: 17 March 2025

Abstract

In this study, we discuss the influence of carbon support on the performance of platinum nanoparticles (Pt-NPs) in gas-phase CO_2 hydrogenation towards industrially demanding CO production. To this end, Pt-supported on graphite oxide, carboHIPE, activated carbon, multiwalled carbon nanotubes (MWCNT), and graphite of different specific surface areas and degree of graphitization were synthesized with identical loading per unit surface area (25 µg Pt/m^2 of support) to reveal the contribution of the carbon support. All Pt@carbon nanocomposites were selective to CO at temperatures above 800 K, however, we found an additional correlation between their catalytic performance and the degree of graphitization of the support. Graphite-supported platinum (Pt@Graphite) has the highest TOF and the lowest activation energy among the studied nanocomposites due to the increasing electron donation from the carbon support to the Pt nanoparticles, which facilitates CO_2 adsorption on Pt by shifting its d-band centre towards the Fermi level. Our study shows that beside surface area, porosity, thermal stability, a further parameter needs to be taken into consideration, as the Pt/C interface has significant effect at the atomic level on the activity of carbon-supported catalysts in gas-phase CO_2 hydrogenation towards CO production.

✉ András Sápi
sapia@chem.u-szeged.hu

[1] Department of Applied and Environmental Chemistry, University of Szeged, Rerrich Béla tér 1, H-6720 Szeged, Hungary

[2] Department of Technology, Faculty of Engineering, University of Szeged, Address 2 Mars tér 7, Szeged 6724, Hungary

[3] Department of Technology, Faculty of Engineering Department of Polymer Chemistry and Technology, National Institute of Chemistry, Hajdrihova ulica 19, 1001 Ljubljana, Slovenia

[4] Department of Molecular and Analytical Chemistry, University of Szeged, Dóm tér 7, Szeged H-6720, Hungary

[5] HUN-REN Reaction Kinetics and Surface Chemistry Research Group, Rerrich Béla tér 1, H-6720 Szeged, Hungary

[6] Grupo Química Básica, Aplicada y Ambiente - Alquimia. Facultad de Ciencias Exactas y Aplicadas. Instituto Tecnológico Metropolitano, Medellín, Colombia

Graphical Abstract

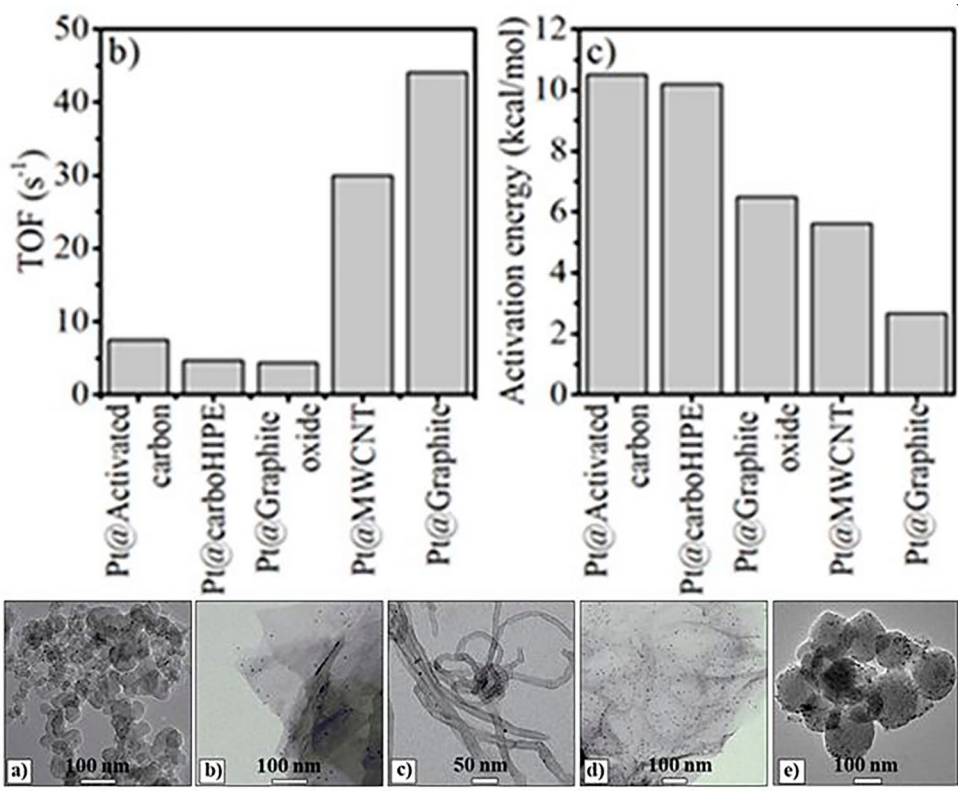

Keywords CO_2 hydrogenation · Carbonaceous supports · Graphitic nature · Pt nanoparticles · RWGS

1 Introduction

The development of a sustainable economy requires a balance between the ecological, social, and economic goals within social and industrial processes. In terms of the IPCC (Intergovernmental Panel on Climate Change) [1], Carbon Dioxide Removal alternatives are needed to compensate for residual emissions from a likely climate overshoot of the targets set in the Paris Agreement. At the industrial level, there is a portfolio of mitigation alternatives with varying levels of development and feasibility. They can be divided into three strategies: reduced GHG (greenhouse gas) emissions, CO_2 Capture and Storage (CCS), and CO_2 utilization [2]. CO_2 utilization processes chemically alter the CO_2 molecule, unlike other technologies that aim to reduce overall CO_2 emissions while leaving the molecule unchanged [3]. CO_2 utilization processes have emerged as a potential complement to CCS and have a promising competitive advantage for a more sustainable industry. A variety of products (e.g., fuels, chemicals or materials) can be synthesized via CO_2 utilization by the appropriate technologies [4]. One such example is the so-called Power-to-Gas (PtG) technology, which uses H_2 and CO_2 to produce alternatives to natural gas [5]. However, this technology still faces many challenges, such as sustainable H_2 production, efficient CO_2 capture from industrial waste streams, and scaling. Nevertheless, these low- and negative-emission technologies can provide an alternative to reduce the exploitation of fossil energy sources and reduce the environmental impacts associated with energy consumption [6].

A CO_2 recycling process requires catalytic reduction into various products, mainly methane, carbon monoxide, and methanol. Afterwards, these products can be further converted into other chemicals through additional steps such as the Fischer–Tropsch process [7]. Typically, the optimization of the CO_2 reduction process is a balance between the endothermic Reverse Water Gas Shift Reaction (RWGS) and the thermodynamically favorable CH_4 formation by the Sabatier process. The key reactions for these processes are listed below:

Reverse water gas shift reaction (RWGS)

$$\begin{aligned} &CO_2 + H_2 \rightarrow CO + H_2O \\ &\Delta H_{298\ K} = 41.2\ kJ/mol \qquad \Delta G_{298\ K} = 28.6\ kJ/mol \end{aligned} \tag{1}$$

Methane formation

$$CO_2 + 4H_2 \rightarrow CH_4 + 2H_2O$$
$$\Delta H_{298\ K} = -252.9\ kJ/mol \qquad \Delta G_{298\ K} = -113.5\ kJ/mol \tag{2}$$

Methanol formation

$$CO_2 + 3H_2 \rightarrow CH_3OH + H_2O$$
$$\Delta H_{298\ K} = -49.5\ kJ/mol \Delta G_{298\ K} = 3.8\ kJ/mol \tag{3}$$

Pt, Cu, and Rh have been identified as the most efficient catalysts for the RWGS reaction, and several key parameters have been found to enhance the catalytic performance. A recently demonstrated example is the synergistic effect between Pt nanoparticles and different substrates (SiO_2 and TiO_2) [8], and another example is the probable correlation between the catalytic activity of industrial catalysts ($Cu/ZnO/Al_2O_3$) for methanol synthesis and the density of defects and twin boundaries [9, 10]. However, explaining catalytic performance still poses a challenge, as for the detailed mechanistic understanding morphology must be taken into account besides the thermodynamic processes involved at given reaction conditions. For example, the reversible migration of zinc atoms towards the copper surface at high temperatures, the partial reduction by the hydrogen reactant, and the role of supports and defects have been reported in the literature [10, 11]. In recent years, various metal@carbon nanocomposites, for instance Pt [12–17], Fe[18], Ni–ZrO_2 [19] or Ni–SiO_2 [20] nanoparticles to name a few, have been investigated for electrocatalytic applications, CO_2 hydrogenation or Fischer–Tropsch catalysis.

To investigate the influence of carbon supports in the gas-phase CO_2 hydrogenation reaction, we prepared and studied Pt@carbon nanocomposites based on different carbonaceous matrices, such as carbon nanotubes, graphite, activated carbon, graphite oxide, and carboHIPE. These supports differ mostly by the degree of graphitization and the specific surface area. The loading of the controlled size Pt-NPs was set to 25 μg/m^2 of carbon support, and significant differences were found in the catalytic activity between samples. Turnover frequencies (TOF) and activation energies reveal the strong influence of the carbonaceous matrix on the performances of the Pt@carbon nanocomposites. It was found, that higher carbon graphitization degree leads to higher TOF values, whereas the overall CO_2 consumption rate strongly depends on the specific surface area.

2 Experimental Section

2.1 Carbon Materials

Activated carbon was purchased from Sigma-Aldrich and used as-received without any further modification. CarboHIPE support was produced as described elsewhere [21]. Briefly, for the preparation of carboHIPE, first, the polyHIPE precursor was synthesized through oil-in-water (O/W) high internal phase emulsion (HIPE) consisting of aqueous solution as the minority phase and toluene as the majority phase. The aqueous solution was composed of acrylamide (AAM, Sigma-Aldrich), N,N′-methylene(bisacrylamide) (MBAM, Sigma-Aldrich), surfactant (Pluronic F-127), ammonium persulfate (APS, Fluka), and N,N,N′,N′- tetramethylethylenediamine (TEMED, Sigma-Aldrich). Once the AAM-based polyHIPE was obtained, the carbonization of the purified polyHIPE was performed in a tube furnace, reaching 900 °C at a heating rate of 5 °C min^{-1}.

For the synthesis of graphite-oxide, 4.5 g graphite powder (Sigma-Aldrich) was sonicated in 210 ml cc. Sulphuric acid (Molar) for 20 min. After sonication and during vigorous mixing, 4.5 g $NaNO_3$ was added to the suspension. After 30 min the suspension was placed on an ice bath, while 27 g potassium-permanganate was slowly added to the slurry. After 24 h of mixing, first 500 ml of distilled water, then 10 ml 50% H_2O_2 was added to the mixture. After 2 h of mixing, the product was washed and collected by centrifugation.

Multiwall carbon nanotubes were produced by CCVD using acetylene precursor and alumina supported 2.5–2.5% iron-cobalt bimetallic catalyst. The system was heated to 700 °C under nitrogen atmosphere in a tube reactor, then C_2H_2:N_2 mixture of 1:9 ratio with a total flow rate of 300 ml min^{-1} was introduced for 30 min. After cooling down in pure N_2 atmosphere, the as-obtained material was suspended in NaOH solution to remove the alumina support, then washed with distilled water. The metal catalyst particles formed at the beginning of the synthesis procedure were dissolved in diluted nitric acid solution. The amorphous carbon was removed by potassium permanganate in acidic media. Carbon nanotubes were finally washed with distilled water to neutral pH and dried in air.

2.2 Synthesis of Size-Controlled Pt Nanoparticles

50 mg H_2PtCl_6 and 220 mg polyvinylpyrrolidone (PVP, MW = 40.000) were dissolved in 10 mL ethylene–glycol and sonicated for 30 min to get a homogeneous solution [22]. The flask was evacuated and purged with atmospheric pressure argon gas. After three purging cycles, the flask was immersed into an oil bath and heated to 433 K for 60 min under vigorous stirring. After reaction, the flask was cooled down to room temperature and sonicated with acetone. After precipitation the particles were washed by centrifugation (6000 RPM, 10 min) with a mixture of 2 mL ethanol and 8 mL hexane. Finally, the particles were re-dispersed in ethanol.

2.3 Catalysts Preparation

To unveil the effect of the carbonaceous support, nanocomposite catalysts with identical platinum (Pt)-nanoparticles per unit surface area loading needed to be prepared. For the preparation of Pt-carbon (Pt@C) nanocomposites, 500 mg of each carbon support was sonicated in 40 mL ethanol to obtain a suspension. A precise volume of platinum was added to the suspension of carbon material from a 1500 ppm ethanol suspension of size-controlled Pt nanoparticles (4–5 nm) to reach 25 µg m^{-2} Pt loading.

2.4 Catalytic Activity Tests

For the catalytic experiment, a 60 min long pretreatment was applied at 573 K with 40 mL min^{-1} of hydrogen flow for all samples. After the pretreatment, the catalyst was cooled down to 473 K and allowed to settle for 5 min in continuous N_2 flow. The gas source was switched to a premixed CO_2:H_2 flow with the constant molar ratio of 1:4 (10:40 mL min^{-1}). The reaction started at 473 K, then the system was heated up to 873 K in 160 min. The CO_2 conversion to CO and CH_4 was detected at temperatures higher than 673 K.

2.5 Characterization

The as-prepared catalysts were characterized by Transmission Electron Microscopy (TEM, FEI Tecnai G^2 20 X-TWIN operated at 200 kV). Raman spectra were collected with a Bruker Senterra II Raman microscope equipped with a 532 nm excitation laser in backscattering configuration. The crystalline structure of the materials was examined by X-ray Diffraction (XRD, Rigaku MiniFlex II Desktop Diffractometer with a CuKα source (λ = 0.1542 nm) operated at 30 kV and 15 mA). Surface areas were determined by nitrogen sorption measurements using a Quantachrome NOVA 3000e instrument and calculated using the Brunauer–Emmett–Teller (BET) model. Thermogravimetric analysis was conducted in a TA Instruments, Q500 instrument using platinum sample holder under oxidative and inert atmospheres (synthetic air and nitrogen, respectively) at a heating rate of 5 K min^{-1}.

The Pt loading of the obtained catalysts was determined by inductively coupled plasma mass spectrometer (ICP-MS) using an Agilent 7900 instrument. 5 mg of each sample was digested in 5 ml high-purity aqua regia (made of ICP-MS grade cc. HNO_3 and cc. HCl) for 4 h at 75 °C. The samples were shaken several times during digestion to aid platinum dissolution. After cooling, 4 ml of the digested mixture was filtered using 0.45 um PES membrane filters and was brought to volume in a 100 ml volumetric flask with deionized water. The platinum concentration of the appropriately diluted aliquots was measured, where each aliquot contained 0.1 ppm mixture of rare earth elements (Aristar, VWR Chemicals) used as internal standards. The ^{194}Pt, ^{195}Pt, and ^{196}Pt isotopes were used for quantification, based on a 11-point calibration series in the 0–100 ppb range (Aristar, VWR Chemicals). Ion counts were measured both with and without a helium collision cell.

XPS spectra were recorded in a Kratos XSAM 800 X-ray photoelectron spectrometer. Double sided carbon tape was used to stick 50 mg sample to a stainless-steel sample holder. The Al Kα x-ray source was operated at 120 W (12 kV). During measurement no sample charging was observed. Survey and high-resolution spectra (C 1 s, O 1 s, and Pt 4f) were collected with a pass energy of 80 and 40 eV, and a step size of 1 and 0.1 eV, respectively. The data was evaluated in the CasaXPS software package [23], where high resolution spectra were corrected with a Shirley background and the aliphatic component of the C 1 s spectra were used as an inner reference at 284.8 eV binding energy. Peaks characteristics of metallic Pt were fit with an asymmetric Lorentzian peak shape (LA(1.2,85,70)).

3 Results and Discussion

3.1 Characterization of Pt@C Nanocomposites

Various carbon matrices, namely graphite oxide, carbo-HIPE, activated carbon, MWCNT, and graphite were used as supports for the Pt-NPs, and the microstructure of the Pt@carbon nanocomposites was characterized by electron microscopy. The TEM images of the nanocomposites in Fig. 1a–e reveal a uniform distribution of 5.0 ± 0.6 nm Pt-NPs (Fig. 2) without any apparent particle aggregation.

Since the catalytic activity of the Pt@carbon nanocomposites was tested as a function of different carbon supports, carbon matrices were characterized by X-ray diffraction (XRD), Raman spectroscopy and N_2-physisorption in detail before any CO_2 hydrogenation reaction. Figure 2 shows the X-ray diffraction (XRD) pattern of the different carbon supports. The diffraction peaks around 26° and 43° 2-theta (2Θ) indicate the crystalline nature of the graphitic structure for the graphite and graphite oxide supports. The other carbon supports show only one broad reflection at about 23° (2Θ), which is likely due to their amorphous structure.

Since catalytic CO_2 hydrogenation was carried out at temperatures above 673 K, the thermal stability of the carbon matrix is of paramount importance. Thus, thermal gravimetric analysis (Figure S1) and high-temperature Raman spectroscopy (Figures S2–6) were carried out. Thermal stability in an oxidative atmosphere (synthetic air) at temperatures up to 873 K showed that MWCNTs and graphite are the

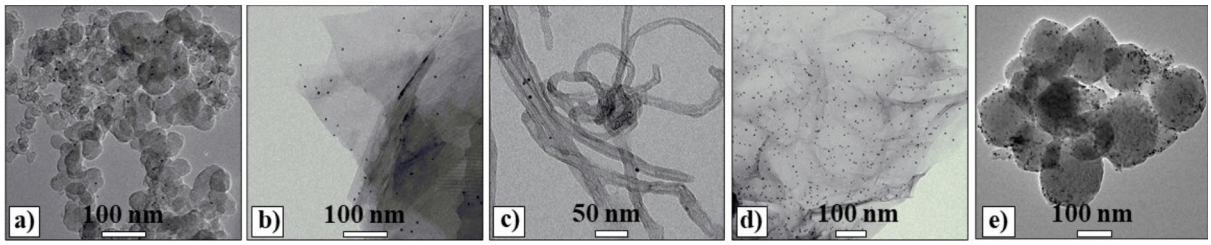

Fig. 1 Platinum nanoparticles on **a** activated carbon, **b** graphite, **c** MWCNT, **d** graphite oxide, **e** carboHIPE

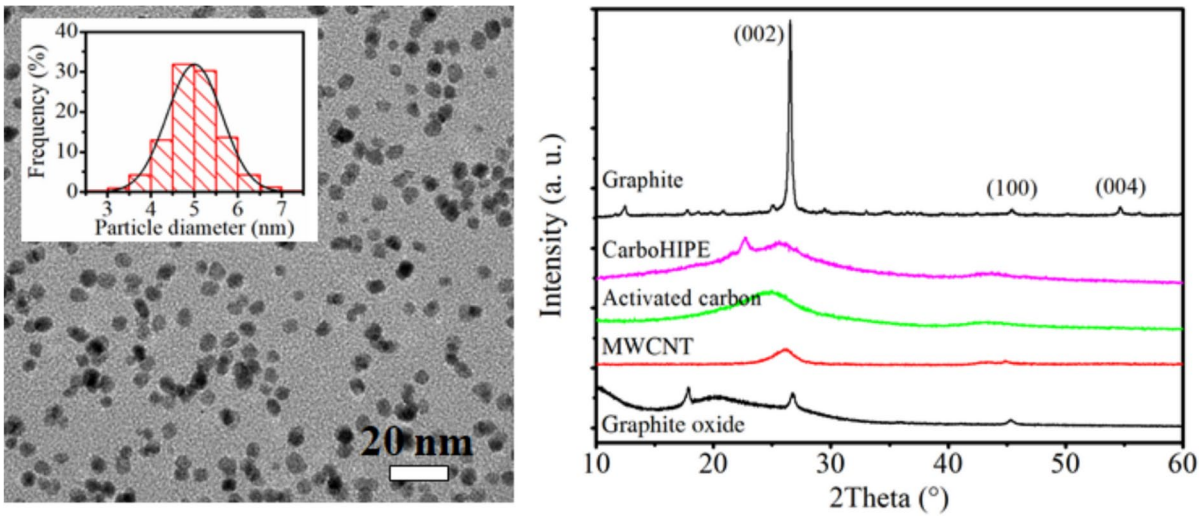

Fig. 2 Size-controlled platinum nanoparticles with a diameter of 5.0±0.6 nm, along with the corresponding particle size distribution in the inset (left), and XRD pattern of the carbon supports (right)

most stable carbon supports. Their decomposition started at about 823 K in good agreement with previous reports [24]. Activated carbon proved to be a moderately stable support, remaining stable up to temperatures above 773 K. Finally, the lowest thermal stability was found for graphite oxide and carboHIPE, where decomposition occurred at around 673 and 700 K, respectively (Figure S1). The high thermal stability of MWCNTs was confirmed by Raman spectroscopy, revealing thermal expansion without any sign of degradation (Figure S4). On the other hand, even though TGA indicated the superior thermal stability of graphite among carbon matrices, Raman spectra show signs of degradation. The intensity of the otherwise weak vibrational band at 643 cm^{-1} increases with temperature above 523 K, which is likely to be related to more pronounced C-H bending deformations (Figure S3). In Pt@activated carbon and Pt@graphite oxide a monotonic increase in I_D/I_G ratio is seen as a sign of degradation. Activated carbon (Figure S2) and graphite oxide (Figure S5) have similar Raman spectra, as both have D and G bands located at 1345 and 1585 cm^{-1}, respectively. In addition, graphite and MWCNTs have similar Raman spectra with an intense peak around 1580 cm^{-1} (G), which is the first-order high-frequency E_{2g} mode. Furthermore, these two carbon matrices show lines corresponding to second-order frequency modes of D', G', D+G, and 2D vibrational bands, and have not been found in other samples (Figure S3 and S4). The lowest signal-to-noise ratio was found for the carboHIPE sample as this carbon matrix emits intense fluorescence during Raman measurements, even when 785 nm laser excitation was used. Nevertheless, Figure S6 confirms the presence of D and G bands at around 1328 cm^{-1} and 1590 cm^{-1}, respectively.

Raman spectroscopy is known as a versatile technique to study defects and the degree of graphitization in carbon materials, and can be used to determine the number of defect sites in carbon supports [25]. The G-band is attributed to sp^2 hybridized carbon, while the D-band is associated with disordered carbon. It is known that the intensity of the D-band increases as the number of defects in the carbon matrix increases. Thus, we have calculated the intensity ratio of the two bands (I_D/I_G) and use this value as an indicator of the change in defect site density. I_D/I_G ratios of 0.65, 1.24, 5.09, and 9.42 were found for graphite, MWCNT, graphite oxide, and activated carbon, respectively. No exact I_D/I_G ratio could be obtained for carboHIPE due to the low signal-to-noise ratio of its spectrum. Hence, the defect site density increases in the following order: graphite<MWCNT<Graphite oxide<Activated carbon.

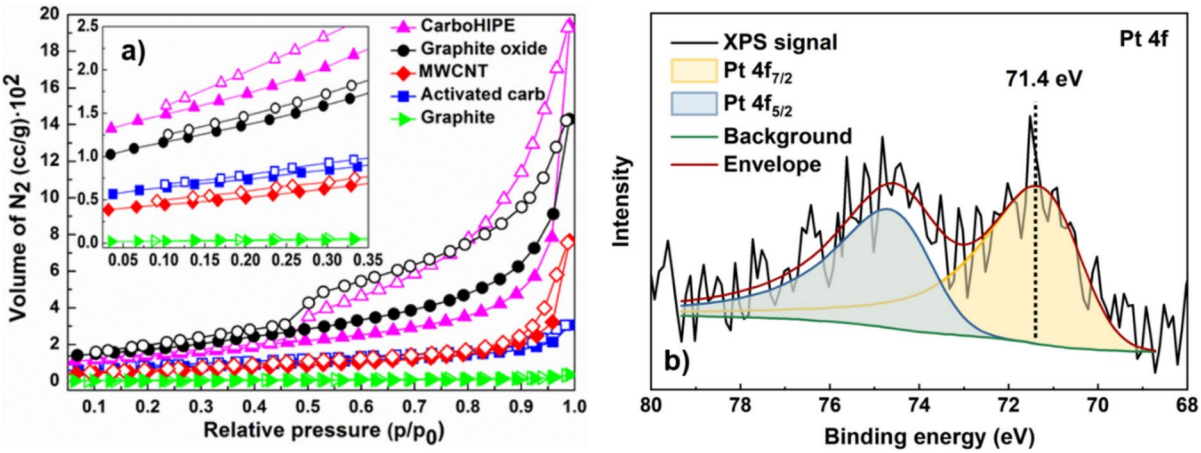

Fig. 3 N_2 sorption isotherms measured at 77 K. The inset shows N_2 uptake in the low relative pressure range ($P/P_0 < 0.35$) (**a**), and the high-resolution XPS spectrum of Pt 4f of Pt/carboHIPE fitted with asymmetric peak shapes for elemental platinum (**b**)

Table 1 Specific surface area (SSA), I_D/I_G ratio characterizing defect density, crystallite size from Eq. 4 and the Scherrer-equation, catalytic performance (TOF at 873 K, CO_2 consumption rate), and the Specific Degree of Graphitization (SGD) index defined in this study

Sample	SSA	I_D/I_G	La	Crystallite size	Pt (ICP-MS)	$TOF_{873\,K}$	Consumption rate	SGD Index
	(m^2/g)		(nm)	(nm)	(w/w %)	(s^{-1})	($nmol/m^2/s$)	(nm/m^2)
Pt@Activated carbon	255	9.42	2.04	1.22	0.68	7.45	35.16	0.0096
Pt@CarboHIPE	266	–	–	0.78	0.69	4.67	13.10	0.0059
Pt@Graphite oxide	624	5.09	3.77	1.36	1.57	4.35	20.53	0.0044
Pt@MWCNT	194	1.24	4.10	3.81	0.51	30.00	87.64	0.0393
Pt@Graphite	11	0.65	29.69	31.42	0.03	44.04	206.61	5.7130

In heterogeneous catalysis the use of porous supports is favorable, as the catalytically active metal centers can be distributed over a larger surface area, which, in turn, leads to higher catalytic performances. Porosity of the Pt@carbon nanocomposites was characterized by the specific surface areas (S_{BET}) calculated from the corresponding nitrogen adsorption/desorption isotherms. Results in Fig. 3 show typical IUPAC type-IV adsorption/desorption behavior with pronounced H3 hysteresis loops. The latter confirms the broad pore size distribution over the micro-, meso- and macropore ranges [26, 27]. The steep increase in N_2 uptake at low relative pressures ($P/P_0 < 0.1$) in carboHIPE, graphite oxide, MWCNT, and activated carbon (Fig. 3 inset) and the hysteresis loops at higher pressures ($0.5 < P/P_0 < 0.8$) in graphite oxide, carboHIPE, and to some extent in MWCNT, are features of micro- and meso-porous structures, respectively The steep increase at $P/P_0 \approx 1$, on the other hand, indicates the presence of macropores in carboHIPE. The specific surface area was calculated using the BET method, and values for S_{BET} were found to be 624, 266, 255, 194, and 11 $m^2\ g^{-1}$ for graphite oxide, carboHIPE, activated carbon, MWCNT, and graphite, respectively. Graphite showed a significantly lower S_{BET} of 11 $m^2\ g^{-1}$ than the other carbon matrices, which can be attributed to the negligible micropore volume. This is further confirmed by the almost zero N_2 uptake at $P/P_0 < 0.1$ (Fig. 3 inset).

Based on the foregoing S_{BET} values of the carbon supports of various graphitization, size-controlled 4–5 nm Pt nanoparticles were deposited to reach 25 µg m^{-2} Pt loading, i.e., 1.536, 0.661, 0.633, 0.483, and 0.027 wt% platinum on carbon for graphite oxide, carboHIPE, activated carbon, MWCNT, and graphite, respectively. The actual Pt loadings were determined by ICP-MS and loadings of 1.568, 0.692, 0.678, 0.509, and 0.032 wt% were obtained on GO, carboHIPE, AC, MWCNT, and graphite-supported catalysts, respectively (Table 1).

The Pt 4f XPS spectrum of the Pt/carboHIPE sample is plotted in Fig. 3b. The binding energies of 71.4 eV and 74.7 eV of the single platinum species are in good agreement with those found for $4f_{7/2}$ and $4f_{5/2}$ of the Pt^0 state in bulk platinum [28]. Oxidized Pt species have slightly higher binding energies of around 75 and 78 eV for $4f_{7/2}$ and $4f_{5/2}$ of Pt(IV) in PtO_2 or $Pt(OH)_4$ [29]. The valence of platinum in Pt NPs depend, among others, on the synthesis route., where by varying the precursor and the reduction process, Pt NPs of different Pt(0)/Pt(IV) [30] or even Pt(0)/Pt(II)/Pt(IV) ratios [31] were obtained. Our polyol synthesis route, on the other hand, provides highly metallic Pt NPs, as we already pointed out by depositing Pt NPs onto hexagonal boron-nitride and SBA-15 supports. Here, no significant charge transfer occurs between the platinum nanoparticles and the support, and hence, the inherent highly metallic state

of the particles was seen [32]. Supports can also modify the initial valence of a metal nanoparticle, and Pt NPs are more metallic on more electrophilic supports or using more electrophilic additives [33]. Studies showed that platinum on acidic supports is less oxidized than on basic ones under an oxidizing atmosphere, whereas in a reducing environment Pt is more electron-deficient on acidic supports [34]. Earlier, we deposited our Pt NPs onto NiO, where Pt got partially oxidized, while operando NAP-XPS measurements showed that during CO_2 hydrogenation at 673 K the oxidized Pt fraction decreased. After the reaction the Pt(δ+) content regained due to oxygen transfer between NiO and the Pt [35]. Although surface oxygen can be found on the Pt (111) surface under pure CO_2 atmosphere at room temperature by ambient pressure XPS, it was removed by the presence of hydrogen and the increase in temperature under reaction conditions. Above 500 °C RWGS reaction prevailed, and surface -OH and H_2O were solely found on the platinum surface. In our study, we performed a reduction step in flowing hydrogen at 573 K for 60 min (see 'Experimental Section') before every test run, and under the reaction conditions used throughout our study, the presence of surface oxygen is highly unlikely. Furthermore, carbon supports possess poor activity in acid-catalyzed reactions, and can be made active only by, e.g., sulfonation or similar chemical process [36]. Since our carbonaceous materials were not activated but used as-prepared, no solid acid-related oxidation state change is expected.

3.2 Hydrogenation Reaction Over Different Pt@C Based Nanocomposites

All Pt@carbon nanocomposite catalysts were activated *in-situ* in a pure H_2 feed at 573 K before being tested in the CO_2 hydrogenation reaction at up to 873 K. The catalytic performances of the Pt@carbon nanocomposites were evaluated based on their selectivity, CO_2 consumption and conversion rate, activation energy, and TOF. The reaction conditions were adjusted so that we achieved relatively low conversion rates, i.e., far from the thermodynamic equilibrium. This ensures that the reported rates correspond to the intrinsic specific activity of the metal catalysts. The conversion rate is expressed as nanomoles of carbon consumed per gram of catalyst per second ($nmol \cdot g^{-1} \cdot s^{-1}$).

Figure 4 plots the CO_2 consumption rate at different temperatures (Fig. 4a) and the isotherms at 873 K (Fig. 4b) for CO_2/H_2 (1:4 ratio). An increase in catalyst activity with increasing reaction temperature is observed for all Pt@carbon nanocomposites, reaching its maximum at 873 K with CO_2 consumption rates of 17,000, 12,813, 8,965, 3,415, and 2,272 $nmol \cdot g^{-1} \cdot s^{-1}$ for Pt@MWCNT, Pt@Graphite oxide, Pt@activated carbon, Pt@carboHIPE, and Pt@graphite, respectively. However, all catalysts showed relatively low catalytic activity at temperatures below 673 K, as their corresponding CO_2 consumption rates were below 1200 $nmol \cdot g^{-1} \cdot s^{-1}$ (Fig. 4a). Interestingly, the CO_2 consumption rates of Pt@graphite and Pt@carboHIPE are reasonably similar (Fig. 4b), although the latter has a significantly larger S_{BET} compared to that of the former. It seems that other variables and the poor thermal stability of carboHIPE are crucial factors for the low CO_2 consumption rate at 873 K compared to the other carbon matrices with similarly high S_{BET}.

Another important observation is, that Pt@carbon nanocomposites show different selectivity for CO and CH_4 (Fig. 5), indicating an important role of the carbon support in the adsorption and dissociation of CO_2. Pt@Graphite oxide and Pt@MWCNT nanocomposites showed 100% selectivity for CH_4 (methanation reaction), despite the lower CO_2 consumption rates at 630 K. With an increasing temperature CH_4 selectivity starts to decrease and levels off at almost 0% above 750 K. Surprisingly, in parallel to that, both samples reach 100% selectivity for CO (RWGS reaction) at temperatures above 750 K (Fig. 5a, b). A reversed trend is observed in Pt@Activated carbon and Pt@carboHIPE, where the nanocomposites showed higher selectivity towards CO, but only slightly increasing selectivity towards CH_4 at higher temperatures. It should be noted that selectivity towards

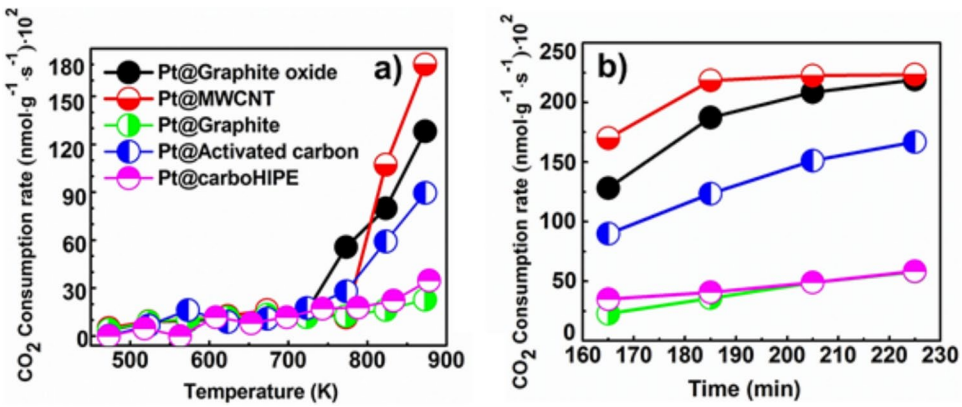

Fig. 4 CO_2 consumption rate of various Pt@carbon nanocomposites at different temperatures (**a**), and time on stream study at 873 K (**b**)

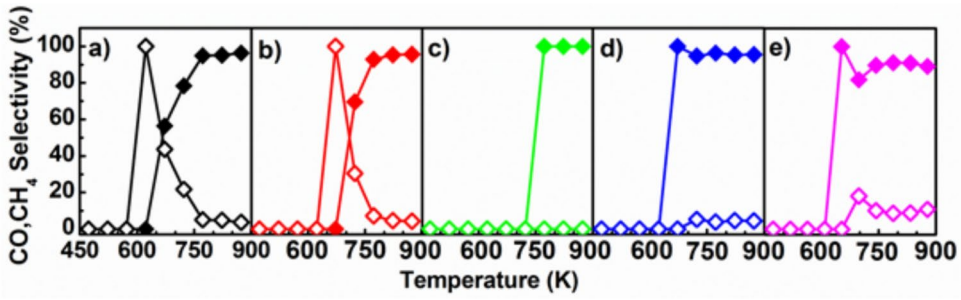

Fig. 5 Selectivity (♦ CO; ◊ CH_4) for the catalysts under review: **a** Pt@Graphite oxide, **b** Pt@MWCNT, **c** Pt@Graphite, **d** Pt@Activated carbon, and **e** Pt@carboHIPE

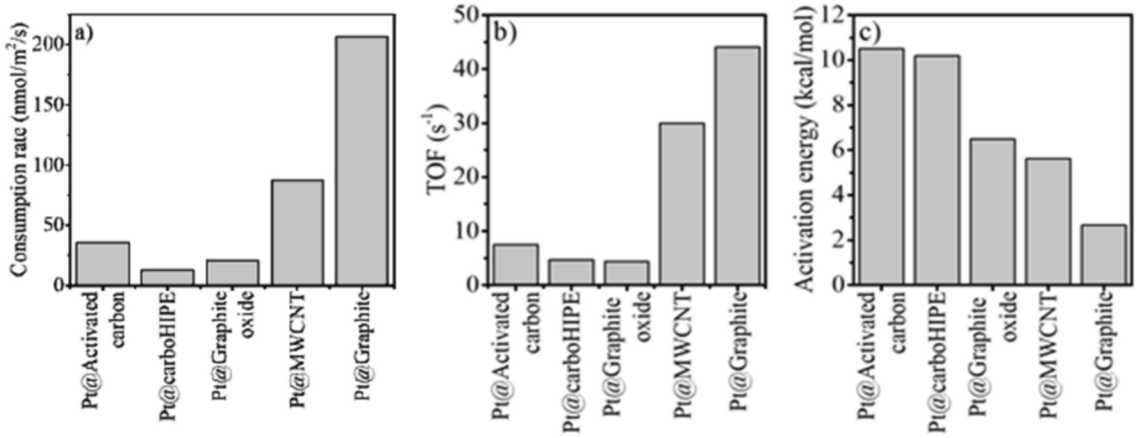

Fig. 6 CO_2 hydrogenation performance of the evaluated catalysts. **a** Consumption rate at 873 K, **b** TOF calculated at 873 K, and **c** activation energy

CH_4 remains low with increasing temperature for Pt@Activated carbon and Pt@carboHIPE, and reaches only 8% and 15% above 750 K, respectively (Fig. 5d, e).

It is known from the literature, that the number of defect sites in a carbon support can affect its catalytic performance, as larger number of defect sites allows for higher CO_2 adsorption capacity [37]. Similarly, the defects within the carbon matrix can also act as anchoring sites for Pt-NPs, allowing for its better dispersion on the surface of the support. This, in turn results in larger Pt-to-carbon interface, which then enhances the reaction with CO_2 to form CH_4 after dissociation of H_2 on the Pt surface [38]. In addition, it is possible to determine the degree of graphitization for each carbon support from Raman spectroscopy. The calculation is based on the ratio of the integral intensity of the D band and the G band, and it is suitable for any laser line in the visible range [39]. Moreover, the general equation developed by Cancado et al. (2006) can be used to describe the crystallite size (La):

$$La\,(nm) = 2.4 \cdot 10^{-10} \cdot \lambda^4 \cdot \frac{1}{I_D/I_G} \tag{4}$$

Good agreement was found with crystallographic studies (Table 1) and has recently been used to characterize the carbon-platinum interface [24]. Additional characterization for the catalysts after reaction has been included in the supporting information.

To compare the catalytic performance of Pt@C nanocomposites, turnover frequency (TOF) values, defined as the number of moles consumed per active Pt site per unit time, at 673 K and 873 K were calculated and plotted in Fig. 6b. Here, the entire surface area is considered available and each atom on the surface is considered as an active site. Our experimental design with fixed loadings of Pt nanoparticles per m^2 result in a fixed number of active sites per nm^2 and it allows a clearer evaluation of the Pt@carbon interface. The number of Pt-NPs available at the surface of the nanocomposite is obtained from the size of the Pt nanoparticles and the amount of Pt added during the preparation of the catalysts. The number of active sites is calculated using the value 0.1521 $nm^2/2$ atoms. Finally, the CO_2 consumption rate is divided by the number of active sites calculated and represents the number of molecules reacting per active site per second (Fig. 6a). One order of magnitude difference in $TOF_{873\ K}$ was found between graphite oxide and graphite. The activation energy was also calculated for each catalyst (Fig. 6c), which showed good agreement with the TOF results of 2.65, 5.62, 6.48, and 10.51 kcal/mol for Pt@Graphite, Pt@MWCNT, Pt@Graphite oxide, and Pt@Activated carbon, respectively. Similarly, the activation energy for graphite was 3.8 times lower than that for activated carbon.

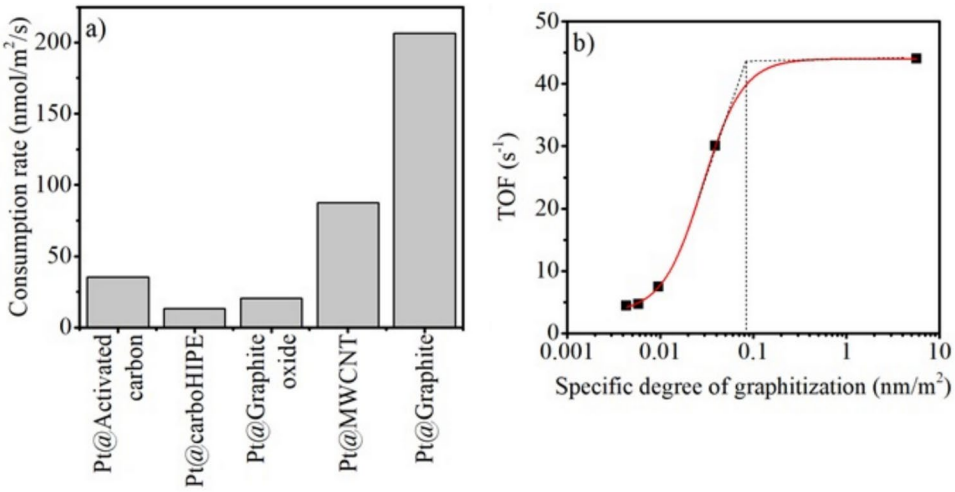

Fig. 7 **a** Consumption rate at 873 K for the evaluated catalysts and **b** TOF vs specific graphitization degree

The large differences in TOF values can be explained by the degree of graphitization (Fig. 6b). The results show that the low degree of graphitization is related to lower activity (TOF_{873K} for Pt@Graphite oxide = 4.35), while higher graphitization led to higher turn-over frequencies of 30 and 44 s^{-1} for MWCNT and graphite, respectively. The number of layers in graphitic samples have a strong correlation with their electronic properties [40]. Therefore, it is expected that the polarization of the Pt-NPs varies due to the charge transfer between the Pt clusters and the graphitic substrates. Density functional theory calculations by Ramos-Sanchez et al. (2013) describes the polarization process for Pt-NPs (~ 1 nm diameter) on graphite. Platinum atoms at the interface are positively charged, while the upper superficial layers carry negative charges, inducing clear differences in their DOS near the Fermi level along with differing catalytic properties [41]. Similarly, the degree of graphitization has been associated with stability and catalyst activity in electrochemical fuel cells [24]. In optics, Sasaki and Hitachi (2020) recently demonstrated the influence of the number of layers on light absorption. As a conclusion, N-layered graphitic materials with N > 1500 can be considered as graphite in light absorption from the infrared to the visible range [42].

As described in the experimental section, the nanocomposite catalysts contain a fixed loading of 25 µg m^{-2} Pt NPs per unit surface area of the carbon support. Thus, the number of Pt-NPs varies between samples depending on the surface area of the carbon support. Figure 7a shows consumption rates that are proportional to the amount of Pt-NPs, which better explains the trends observed in Fig. 6.

Finally, we propose the so-called 'Specific Degree of Graphitization (SDG)' as a characteristic of the Pt-C interface in heterogeneous catalytic reactions. The SGD index is defined as the ratio between the crystallite size obtained by the Scherrer equation from the graphitic peak (corresponding to the (002) reflections), and the surface area

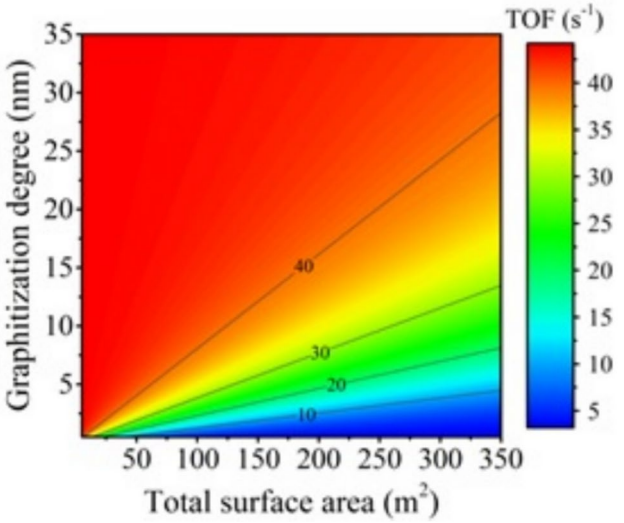

Fig. 8 Dependence of CO_2 hydrogenation activity of Pt@carbon catalysts on the total specific surface area and the Specific Degree of Graphitization (SDG) of the carbon supports

of the carbon support (crystallite size/surface area in [nm m^{-2}] or [nm^{-1}]). The input data for the calculation and the resulted SDGs are listed in Table 1 and depicted in Fig. 7b in a semi-logarithmic graph by plotting TOF values against the logarithm of the corresponding SDGs of each catalyst on different carbon supports.

The resulted sigmoid-type curve in Fig. 7b was fitted by a logistic function to guide the eye, where the inflection point for high TOF performances of Pt NPs on carbon substrates can be found at SDG ≈ 0.085 nm m^{-2}. To further visualize the carbon support-dependent catalytic performance of the evaluated Pt-NPs@carbon nanocomposites in gas-phase CO_2 hydrogenation, a contour plot was constructed in Fig. 8, where the variation of TOF on the total specific surface area and the graphitization degree can be seen. This representation confirms, that although the specific surface area is an important parameter, detailed description of the

CO_2 hydrogenation activity on carbon supported catalysts cannot be realized without taken the degree of graphitization of the support into consideration. A great example to that is, that although the graphite-based catalyst had the lowest S_{BET} (Table 1), it showed the highest TOF value in our study as shown in Fig. 7b and 8. Based on the above findings, we propose the use of high surface area carbon supports with an optimal graphite stacking thickness of 30 layers (10 nm thick layer built up from C (002) layers with 0.34 nm plane spacing) for gas-phase CO_2 hydrogenation on Pt@carbon catalysts.

The mechanism of the reverse-gas shift reaction (RWGS) (Eq. 1) is still under scrutiny in the literature, and after the initial CO_2 adsorption step the following three different elementary steps were proposed:

$$CO_2 \rightarrow CO + O \quad (5)$$

$$CO_2 + H \rightarrow COOH \quad (6)$$

$$CO_2 + H_2 \rightarrow HCOO \quad (7)$$

CO_2 hydrogenation seems to follow one of the above pathways depending on the catalyst, the support, and the reaction conditions. It is generally assumed that RWGS proceeds through the carbonate-mediated mechanism on Pt, as CO_2 dissociation is only favorable on metals of high oxygen affinity (Rh, Ni, Cu) and the high stability of the surface formate makes it a spectator group [43]. However, there are contradictory reports on the possible adsorption and dissociation of CO_2 on Pt. Early UHV study demonstrated that CO_2 adsorbs and dissociates on Pt(111) only upon K doping [44], whereas UHV XPS measurements showed the presence of chemisorbed CO on Pt foil [45]. Recent APXPS results found evidence on the adsorption and dissociation of CO_2 to CO on Pt(111) single crystal in the presence and absence of additional H_2 even at room temperature [36].

Catalysts' functionalities can be described by the energetics of the adsorbed species, nevertheless extending the study from well-defined single crystal model systems to supported nanoparticle catalysts is challenging introducing [46]. DFT calculations showed that CO_2 hydrogenation goes entirely through the carbonate pathway, and the low RWGS activity on self-standing Pt NPs is associated with the weak adsorption of CO_2 in the initial step. The latter favors CO_2 desorption before hydrogenation takes place, and thus by stabilizing adsorbed CO_2 on the catalyst surface increases conversion. It is known that catalyst supports can fundamentally influence a catalyst's behavior by, e.g., perturbing the electronic properties of the metal nanoparticle, stabilizing certain surface species etc. For instance, low-coordinated Pt sites at corners and edges adsorb CO_2 primarily, but the weak bonding between these sites and the adsorbate hinders to achieve high activity. Whereas, e.g., surface –OH groups in Pt/SiO_2 or oxygen vacancies in Pt/TiO_2 can enhance CO_2 adsorption on Pt NPs [47]. By choosing the right support the electronic structure of the interface with the catalyst particle can be tailored, too. Electronic metal-support interaction (EMSI) describes chemical bonding and the associated charge transfer at the metal/support interface. This, in turn, charges the metal either negatively or positively, where the resulting electron-rich or electron-deficient surface becomes donor or acceptor for the reactants. Carbon materials are tunable supports, where modulating defect density, surface chemistry (e.g., the density of Electron-Withdrawing Groups (EWG) like ether, carbonyl, and carboxyl, and Electron-Donor Groups (EDG), like hydroxyl), and heteroatom dopants can tailor electron transfer via moving electrons through the π-bonds of the carbon structure (resonance) or bond polarization by electronegativity differences (inductive effect). It is known that adsorption is highly influenced by the energy and filling of metal d-band, and electron transfer from the metal particle to the support shifts the d-band of the metal upward closer to the Fermi level (shallow d band). This results in stronger intermediate-surface interaction [48]. Such strongly surface-bound CO is the origin of CO-poisoning of Pt, which hinders, e.g., the CO oxidation reaction. Several studies investigated the promotion of the latter on Pt using various carbon supports with fine-tuned electronic properties, changing the surface density of defects and oxygen-containing functional groups (OCGs). It was concluded, that increasing EWG/EDG ratio and higher defect density empty and lower the Pt d-band, which weaken the CO–Pt adsorption on the carbon black-carbon nanotube-carbon nanofiber series [[49, 50]], and on carbon nanotubes with tailored EWG/EDG ratio [51]. In our case, for stronger CO_2 adsorption shallower d-band, i.e. filling of the Pt d-bands via electron transfer from the carbon support to the Pt and the corresponding upward shift of the d-band center, is required. It is also known that d-band centers are shallower for higher index Pt surfaces, whose CO_2 adsorption energy is higher than those on planes of lower Miller indices [52]. Moreover, CO_2 weakly physisorbs on uncharged Pt, whereas CO_2 molecule chemisorbs on charged Pt surfaces through partial electron transfer from Pt to the antibonding $2\pi_u$ LUMO to form CO_2^-. This reduces bond strength and bends the CO_2 molecule, and size-dependent CO_2 adsorption on Pt clusters found evidence of both molecular and dissociative adsorptions. It was suggested for practical applications to deposit small Pt clusters onto electron donating supports, like metal oxides or carbon [53]. To that end, a decreasing EWG/EDG ratio needs to be realized by either increasing EDG or decreasing EWG surface density. Here, higher SGD (Table 1) implies

the increase in sp^2/sp^3, which in turn means the decrease of the electron withdrawing potential of the support. Furthermore, Raman results in Figure S2-6 indicated the formation of defect in the carbon supports, which can further stabilize the adsorbed CO_2 molecules at the Pt/C interface, as discussed above [54].

4 Conclusions

Pt supported on graphite oxide, carboHIPE, activated carbon, MWCNT, and graphite were synthesized to investigate the influence of the physicochemical properties of the carbon support on the performance as a nanocomposite catalyst in CO_2 hydrogenation reaction in gas phase. No significant effect of the carbon support on Pt nanoparticle size distribution was seen, as NP size was mainly controlled by the synthesis method. The nanocomposite catalysts were prepared with identical Pt-NPs loading of 25 µg m^{-2} of support and their thermal stability was characterized by TGA and Raman spectroscopy at reaction temperatures. The carbon supports were found to have different amounts of defective sites in the carbon skeleton, as shown by the Raman results, which in turn affect the platinum–carbon interface and the electronic interactions that determine catalytic activity.

A relationship was found between the degree of graphitization of the carbon support and the catalytic performance of the studied Pt@carbon catalysts. We, therefore, defined the so-called Specific Degree of Graphitization (SDG), with which we were able to describe the correlation between the CO_2 hydrogenation activity (TOF at 873 K) and the degree of graphitization of the carbon support in Pt@carbon composites. The highest activity among the investigated catalysts was found for the Pt on graphite nanocomposite, showing a $TOF_{873\,K}$ as high as 44 s^{-1} along with the highest SDG index of 5.7130 nm m^{-2}. The higher CO_2 hydrogenation activity in RWGS originates from the increasing electron donation of the carbon support to the Pt nanoparticles by the increase in graphitization. This, in turn, enhances the rate-limiting initial CO_2 adsorption on Pt by shifting its d-band center towards the Fermi level, demonstrating enhance CO_2 activation. We propose the defined SDG index as a powerful indicator for the prediction of CO_2 hydrogenation catalytic activity on Pt@carbon nanocomposites.

Supplementary Information The online version contains supplementary material available at https://doi.org/10.1007/s10562-025-04989-8.

Acknowledgements AS gratefully acknowledges the support of FK 143583 and ZK is grateful for K_21 138714 project from the source of the National Research, Development and Innovation Fund. The Ministry of Human Capacities through the 20391-3/2018/FEKUSTRAT, as well as Project no. TKP2021-NVA-19 under the TKP2021-NVA funding scheme of the Ministry for Innovation and Technology are acknowledged. Project no. RRF-2.3.1-21-2022-00009, titled National Laboratory for Renewable Energy has been implemented with the support provided by the Recovery and Resilience Facility of the European Union within the framework of Programme Széchenyi Plan Plus. SK acknowledges the financial support from the Slovenian Research Agency (grant P2-0145). JGP acknowledges the financial support from the Administrative Department of Science, Technology, and Innovation of Colombia (Colciencias). HH acknowledges financial support of the János Bolyai Research Grant of the Hungarian Academy of Sciences (BO/682/22) and the MTA Sustainable Development and Technologies National Programme of MTA, Sustainable Technologies Sub-Programme (NP2022-II-7/2022).

Funding Open access funding provided by University of Szeged.

References

1. Masson-Delmotte V, Zhai P, Pörtner H-O, Roberts D, Skea J, Shukla PR, Pirani A, Moufouma-Okia W, Péan C, Pidcock R, Connors S, Matthews JBR, Chen Y, Zhou X, Gomis MI, Lonnoy E, Maycock T, Tignor M, Waterfield T, Intergovernmental panel on climate change-global warming of 1.5 degrees celcius, 2018. https://doi.org/10.1017/CBO9781107415324.
2. Liu M, Yi Y, Wang L, Guo H, Bogaerts A (2019) Hydrogenation of carbon dioxide to value-added chemicals by heterogeneous catalysis and plasma catalysis. Catalysts. https://doi.org/10.3390/catal9030275
3. Aresta M, Dibenedetto A, Angelini A (2013) The changing paradigm in CO2 utilization. J CO2 Util. https://doi.org/10.1016/j.jcou.2013.08.001
4. Styring P, Quadrelli EA, Armstron K (2015) Carbon dioxide utilization: closing the carbon cycle. Elsevier, Amsterdam
5. von der Assen N, Voll P, Peters M, Bardow A (2014) Life cycle assessment of CO2 capture and utilization: a tutorial review. Chem Soc Rev 43:7982–7994. https://doi.org/10.1039/c3cs60373c
6. Rönsch S, Schneider J, Matthischke S, Schlüter M, Götz M, Lefebvre J, Prabhakaran P, Bajohr S (2016) Review on methanation-from fundamentals to current projects. Fuel 166:276–296. https://doi.org/10.1016/j.fuel.2015.10.111
7. Studt F, Abild-Pedersen F, Wu Q, Jensen AD, Temel B, Grunwaldt JD, Norskov JK (2012) CO hydrogenation to methanol on Cu-Ni catalysts: theory and experiment. J Catal 293:51–60. https://doi.org/10.1016/j.jcat.2012.06.004
8. Kattel S, Liu P, Chen JG (2017) Tuning selectivity of CO2 hydrogenation reactions at the metal/oxide interface. J Am Chem Soc 139:9739–9754. https://doi.org/10.1021/jacs.7b05362

9. Greeley JP (2012) Active site of an industrial catalyst. Science 336:810–811. https://doi.org/10.1126/science.1222974
10. Behrens M, Studt F, Kasatkin I, Kühl S, Hävecker M, Abild-Pedersen F, Zander S, Girgsdies F, Kurr P, Kniep BL, Tovar M, Fischer RW, Nørskov JK, Schlögl R (2012) The active site of methanol synthesis over Cu/ZnO/Al2O3 industrial catalysts. Science 336:893–897. https://doi.org/10.1126/science.1219831
11. Sápi A, Dobó DG, Sebok D, Halasi G, Juhász KL, Szamosvölgyi Á, Pusztai P, Varga E, Kálomista I, Galbács G, Kukovecz Á, Kónya Z (2017) Silica-based catalyst supports are inert, are they not?: striking differences in ethanol decomposition reaction originated from meso- and surface-fine-structure evidenced by small-angle X-ray scattering. J Phys Chem C 121:5130–5136. https://doi.org/10.1021/acs.jpcc.7b00034
12. Park S, Xie Y, Weaver MJ (2002) Electrocatalytic pathways on carbon-supported platinum nanoparticles: comparison of particle-size-dependent rates of methanol, formic acid, and formaldehyde electrooxidation. Langmuir 18:5792–5798. https://doi.org/10.1021/la0200459
13. Antolini E (2003) Formation, microstructural characteristics and stability of carbon supported platinum catalysts for low temperature fuel cells. J Mater Sci 38:2995–3005. https://doi.org/10.1023/A:1024771618027
14. Huang X, Long C, Han J, Zhang J, Qiu X, Tang Z (2020) Remarkably enhanced hydrogen oxidation reaction activity of carbon-supported Pt by Facile nickel modification. Chem Res Chinese Univ 36:105–109. https://doi.org/10.1007/s40242-020-9074-9
15. Varga T, Ballai G, Vásárhelyi L, Haspel H, Kukovecz Á, Kónya Z (2018) Co4N/nitrogen-doped graphene: a non-noble metal oxygen reduction electrocatalyst for alkaline fuel cells. Appl Catal B Environ 237:826–834. https://doi.org/10.1016/j.apcatb.2018.06.054
16. Sápi A, Varga A, Samu GFGF, Dobó DG, Juhász KLKL, Takács B, Varga E, Kukovecz A, Kónya Z, Janáky C, Takacs B, Varga E, Kukovecz A, Kónya Z, Janáky C (2017) Photoelectrochemistry by design: tailoring the nanoscale structure of Pt/NiO composites leads to enhanced photoelectrochemical hydrogen evolution performance. J Phys Chem C 121:12148–12158. https://doi.org/10.1021/acs.jpcc.7b00429
17. Bai L, Wang X, Tang S, Kang Y, Wang J, Yu Y, Zhou ZK, Ma C, Zhang X, Jiang J, Chu PK, Yu XF (2018) Black phosphorus/platinum heterostructure: a highly efficient photocatalyst for solar-driven chemical reactions. Adv Mater 30:1803641. https://doi.org/10.1002/adma.201803641
18. Williamson DL, Herdes C, Torrente-Murciano L, Jones MD, Mattia D (2019) N-Doped Fe@CNT for combined RWGS/FT CO2 hydrogenation. ACS Sustain Chem Eng 7:7395–7402. https://doi.org/10.1021/acssuschemeng.9b00672
19. Romero Sáez M, Dongil AB, Benito N, Espinoza-González R, Escalona N, Garcia F (2018) CO2 methanation over nickel-ZrO2 catalyst supported on carbon nanotubes: a comparison between two impregnation strategies. Appl Catal B Environ 237:817–825. https://doi.org/10.1016/j.apcatb.2018.06.045
20. Ma H, Ma K, Ji J, Tang S, Liu C, Jiang W, Yue H, Liang B (2019) Graphene intercalated Ni-SiO2/GO-Ni-foam catalyst with enhanced reactivity and heat-transfer for CO2 methanation. Chem Eng Sci 194:10–21. https://doi.org/10.1016/j.ces.2018.05.019
21. Mazaj M, Bjelica M, Žagar E, Logar NZ, Kovačič S (2020) Zeolite Nanocrystals embedded in microcellular carbon foam as a high-performance CO2 capture adsorbent with energy-saving regeneration properties. Chemsuschem 13:2089–2097. https://doi.org/10.1002/cssc.201903116
22. Sápi A, Kashaboina U, Ábrahámné KB, Gómez-Pérez J, Szenti I, Halasi G, Kiss J, Nagy B, Varga T, Kukovecz Á, Kónya Z (2019) Synergetic of Pt Nanoparticles and H-ZSM-5 zeolites for efficient CO2 activation: role of interfacial sites in high activity. Front Mater 6:1–12. https://doi.org/10.3389/fmats.2019.00127
23. Pinder JW, Major GH, Baer DR, Terry J, Whitten JE, Čechal J, Crossman JD, Lizarbe AJ, Jafari S, Easton CD, Baltrusaitis J, van Spronsen MA, Linford MR (2024) Avoiding common errors in X-ray photoelectron spectroscopy data collection and analysis, and properly reporting instrument parameters. Appl Surf Sci Adv 19:100534. https://doi.org/10.1016/J.APSADV.2023.100534
24. Willinger E, Tarasov A, Blume R, Rinaldi A, Timpe O, Massué C, Scherzer M, Noack J, Schlögl R, Willinger MG (2017) Characterization of the platinum-carbon interface for electrochemical applications. ACS Catal 7:4395–4407. https://doi.org/10.1021/acscatal.7b00614
25. Preuss K, Kannuchamy VK, Marinovic A, Isaacs M, Wilson K, Abrahams I, Titirici MM (2016) Bio-inspired carbon electro-catalysts for the oxygen reduction reaction. J Energy Chem 25:228–235. https://doi.org/10.1016/j.jechem.2016.01.001
26. Kruk M, Jaroniec M (2001) Gas adsorption characterization of ordered organic-inorganic nanocomposite materials. Chem Mater 13:3169–3183. https://doi.org/10.1021/cm0101069
27. Sing KSW, Everett DH, Haul RAW, Moscou L, Pierotti RS, Rouquerol J, Siemieniewska T (1985) Reporting physisorption data for gas/solid systems with special reference to the determination of surface area and porosity. Pure Appl Chem 57:603–619. https://doi.org/10.1351/pac198557040603
28. Qu Y, Sutherland AM, Lien J, Suarez GD, Guo T (2010) Probing site activity of monodisperse Pt nanoparticle catalysts using steam reforming of methane. J Phys Chem Lett 1:254–259. https://doi.org/10.1021/jz900098x
29. Hamnett A, Kennedy BJ, Weeks SA (1988) Base metal oxides as promotors for the electrochemical oxidation of methanol. J Electroanal Chem Interfacial Electrochem 240:349–353. https://doi.org/10.1016/0022-0728(88)80337-1
30. Şen F, Gökagaç G (2007) Activity of carbon-supported platinum nanoparticles toward methanol oxidation reaction: role of metal precursor and a new surfactant, tert-octanethiol. J Phys Chem C 111:1467–1473. https://doi.org/10.1021/JP065809Y/ASSET/IMAGES/LARGE/JP065809YF00009.JPEG
31. Mondal A, Jana NR (2015) Effect of size and oxidation state of platinum nanoparticles on the electrocatalytic performance of graphene-nanoparticle composites. RSC Adv 5:85196–85201. https://doi.org/10.1039/C5RA17087G
32. Hegedűs T, Szenti I, Efremova A, Szamosvölgyi Á, Baán K, Kiss J, Kónya Z (2024) Hexagonal boron nitride fibers as ideal catalytic support to experimentally measure the distinct activity of Pt nanoparticles in CO2 hydrogenation. Heliyon. https://doi.org/10.1016/j.heliyon.2024.e40078
33. Yoshida H, Nonoyama S, Yazawa Y, Hattori T (2005) Quantitative determination of platinum oxidation state by XANES analysis. Phys Scr T T 115:813–815. https://doi.org/10.1238/PHYSICA.TOPICAL.115A00813/XML
34. Grubbs RH, Kroll LRC (1971) Catalytic reduction of olefins with a polymer-supported rhodium(I) catalyst. J Am Chem Soc 93:3062–3063. https://doi.org/10.1021/JA00741A050/ASSET/JA00741A050.FP.PNG_V03
35. Sápi A, Halasi G, Kiss J, Dobó DG, Juhász KL, Kolcsár VJ, Ferencz Z, Vári G, Matolin V, Erdőhelyi A, Kukovecz Á, Kónya Z (2018) In Situ DRIFTS and NAP-XPS exploration of the complexity of co2hydrogenation over size-controlled Pt nanoparticles supported on mesoporous NiO. J Phys Chem C. https://doi.org/10.1021/acs.jpcc.8b00061
36. Su H, Ye Y, Lee KJ, Zeng J, Mun BS, Crumlin EJ (2020) Probing the surface chemistry for reverse water gas shift reaction on Pt(1 1 1) using ambient pressure X-ray photoelectron spectroscopy. J Catal 391:123–131. https://doi.org/10.1016/J.JCAT.2020.08.017

37. Lin Y, Li P, Cui T, Pan X, Bao X (2018) Modulating the CO methanation activity of Ni catalyst by nitrogen doped carbon. J Energy Chem 27:898–902. https://doi.org/10.1016/j.jechem.2017.06.008
38. Rewick RT, Wentrcek PR, Wise H (1974) Carbon gasification in the presence of metal catalysts. Fuel 53:274–279. https://doi.org/10.1016/0016-2361(74)90048-9
39. Cancado LG, Takai K, Enoki T, Endo M, Kim YA, Mizusaki H, Jorio A, Coelho LN, Magalhães-Paniago R, Pimenta MA (2006) General equation for the determination of the crystallite size La of nanographite by Raman spectroscopy. Appl Phys Lett 88:1–4. https://doi.org/10.1063/1.2196057
40. Hibino H, Kageshima H, Kotsugi M, Maeda F, Guo FZ, Watanabe Y (2009) Dependence of electronic properties of epitaxial few-layer graphene on the number of layers investigated by photoelectron emission microscopy. Phys Rev B-Condens Matter Mater Phys 79:1–7. https://doi.org/10.1103/PhysRevB.79.125437
41. Ramos-Sanchez G, Balbuena PB (2013) Interactions of platinum clusters with a graphite substrate. Phys Chem Chem Phys 15:11950–11959. https://doi.org/10.1039/c3cp51791h
42. Sasaki K, Hitachi K (2020) Universal layer number in graphite. Commun Phys 3:1–5. https://doi.org/10.1038/s42005-020-0354-y
43. Dietz L, Piccinin S, Maestri M (2015) Mechanistic insights into CO2 activation via reverse water - Gas shift on metal surfaces. J Phys Chem C 119:4959–4966. https://doi.org/10.1021/JP512962C/SUPPL_FILE/JP512962C_SI_001.PDF
44. Lombardo SJ, Bell AT (1991) A review of theoretical models of adsorption, diffusion, desorption, and reaction of gases on metal surfaces. Surf Sci Rep 13:3–72. https://doi.org/10.1016/0167-5729(91)90004-H
45. Huang M, Adnot A, Suppiah S, Kaliaguine S (1995) XPS observation of surface interaction between H2 and CO2 on platinum foil. J Mol Catal A Chem 104:L131–L137. https://doi.org/10.1016/1381-1169(95)00187-5
46. Calle-Vallejo F, Loffreda D, Koper MTM, Sautet P (2015) Introducing structural sensitivity into adsorption–energy scaling relations by means of coordination numbers. Nat Chem 75:403–410. https://doi.org/10.1038/nchem.2226
47. Kattel S, Yan B, Chen JG, Liu P (2016) CO2 hydrogenation on Pt, Pt/SiO2 and Pt/TiO2: importance of synergy between Pt and oxide support. J Catal 343:115–126. https://doi.org/10.1016/J.JCAT.2015.12.019
48. Sang K, Zuo J, Zhang X, Wang Q, Chen W, Qian G, Duan X (2023) Towards a molecular understanding of the electronic metal-support interaction (EMSI) in heterogeneous catalysis. Green Energy Environ 8:619–625. https://doi.org/10.1016/J.GEE.2022.12.006
49. Chen W, Liu C, Lian C, Yu Y, Zhang X, Qian G, Yang J, Chen D, Zhou X, Yuan W, Duan X (2024) Engineering electronic platinum–carbon support interaction to tame carbon monoxide activation. Fundam Res 4:1118–1127. https://doi.org/10.1016/J.FMRE.2022.06.012
50. Chen W, Cao J, Fu W, Zhang J, Qian G, Yang J, Chen D, Zhou X, Yuan W, Duan X (2022) Molecular-level insights into the notorious CO poisoning of platinum catalyst. Angew Chemie Int Ed 61:e202200190. https://doi.org/10.1002/ANIE.202200190
51. Chen J, Xiong S, Liu H, Shi J, Mi J, Liu H, Gong Z, Oliviero L, Maugé F, Li J (2023) Reverse oxygen spillover triggered by CO adsorption on Sn-doped Pt/TiO2 for low-temperature CO oxidation. Nat Commun 141:1–12. https://doi.org/10.1038/s41467-023-39226-6
52. Wong YJ, Choi YH, Tanaka S, Yoshioka H, Mukai K, Halim HH, Mohamed AR, Inagaki K, Hamamoto Y, Hamada I, Yoshinobu J, Morikawa Y (2021) Adsorption of CO2 on terrace, step, and defect sites on Pt surfaces: a combined TPD, XPS, and DFT study. J Phys Chem C 125:23657–23668. https://doi.org/10.1021/ACS.JPCC.1C05228/ASSET/IMAGES/LARGE/JP1C05228_0008.JPEG
53. Green AE, Justen J, Schçllkopf W, Lexander Gentleman AS, Fielicke A, Mackenzie SR, Green AE, Entleman DS, Mackenzie SR, Justen J, Schçllkopf D (2018) IR signature of size-selective CO2 activation on small platinum cluster anions. Angew Chemie Int Ed 57:14822–14826. https://doi.org/10.1002/ANIE.201809099
54. Bahruji H, Bowker M, Hutchings G, Dimitratos N, Wells P, Gibson E, Jones W, Brookes C, Morgan D, Lalev G (2016) Pd/ZnO catalysts for direct CO2hydrogenation to methanol. J Catal 343:133–146. https://doi.org/10.1016/j.jcat.2016.03.017